

Excitonic Dynamical Franz-Keldysh Effect

K. B. Nordstrom¹, K. Johnsen^{2,3}, S. J. Allen¹, A. P. Jauho², B. Bimir³, J. Kono⁴, T. Noda⁵,
H. Akiyama⁵, and H. Sakaki^{4,5}¹Center for Terahertz Science and Technology, Quantum Institute, University of California,
Santa Barbara, California, 93106, USA²Mikroelektronik Centret, Technical University of Denmark, Bldg 345east
DK-2800 Lyngby, Denmark³Mathematics Department, University of California, Santa Barbara, California, 93106, USA⁴Quantum Transition Project, Japan Sci. & Tech. Corp., Tokyo 153, Japan⁵Institute of Industrial Science, University of Tokyo, Tokyo 106, Japan

The Dynamical Franz-Keldysh Effect is exposed by exploring near-bandgap absorption in the presence of intense THz electric fields. It bridges the gap between the DC Franz-Keldysh effect and multiphoton absorption and competes with the THz AC Stark Effect in shifting the energy of the excitonic resonance. A theoretical model which includes the strong THz field non-perturbatively via a non-equilibrium Green Functions technique is able to describe the Dynamical Franz-Keldysh Effect in the presence of excitonic absorption.

PACS numbers: 78.30.Fs, 78.20.Bh, 78.66.Fd, 71.10.-w, 71.35.Cc

(Draft: March 23, 2024)

We report observation of the Dynamical Franz-Keldysh Effect (DFKE) by examination of the near-bandgap optical properties of a semiconductor multiple quantum well (MQW) in a new experimental regime. By applying a strong electric field at frequencies near 1 THz, we perform electro-absorption spectroscopy which is described by neither the DC Franz-Keldysh Effect (FKE) [1,2], nor by optical-frequency effects like multiphoton absorption (MPA) [3]. The DFKE region, bridging these two extremes, is a topic of longstanding theoretical interest [4-6], but has not previously been studied experimentally.

The crossover between "high" and "low" frequency may be quantified in terms of two parameters, E_{KE} and ω_c , defined as:

$$E_{KE} = \frac{e^2 E_{THz}^2}{4m^* \hbar^2 \omega_c^2} : \quad (1)$$

$$\omega_c = \frac{E_{KE}}{\hbar \omega_{THz}} = \frac{e^2 E_{THz}^2}{4m^* \hbar^3 \omega_{THz}^3} : \quad (2)$$

E_{KE} is the mean kinetic energy of a particle of mass m and charge e in an electric field $E_{THz} \cos(\omega_{THz} t)$, i.e. the ponderomotive energy. The DC FKE corresponds to $\omega_c \ll \omega_{THz}$; multiphoton effects occur for $\omega_c \gg \omega_{THz}$; and the case of $\omega_c \sim \omega_{THz}$ is a new, distinct DFKE regime [4] (Fig. 1). This regime is difficult to access experimentally, as E_{KE} must be comparable to or greater than any broadening energies in the system. However, it is possible for applied fields with $\omega_{THz} \sim 1$ THz and $E_{THz} \sim 1$ 10kV/cm [5].

In this paper, we explore the optical absorption of a semiconductor multiple quantum well (MQW) driven by an intense THz electric field polarized in the plane of the MQW layers. For the case of non-interacting carriers,

the DFKE predicts a blue-shift of the main absorption edge in the spectrum by E_{KE} , as well as increased sub-gap absorption [5] (Fig. 2a). This DFKE blue-shift has not previously been observed.

In order to properly address the DFKE, we must also consider the effect of excitons, which dominate the observed near-bandgap absorption in undoped semiconductors. Excitons are bound states of an electron and hole with hydrogen-like quantized energy levels. The energy level spacings can be in the THz regime. The interaction of excitonic states with a THz field leads to shifts of the levels via the AC Stark Effect [7] (Fig. 2b). The THz field interacts most strongly with the exciton $1s \rightarrow 2p$ transition [8]. We present below a novel theoretical model which shows that the experimentally observed changes in the absorption spectrum, as a function of the THz field intensity and frequency, display the DFKE and its interplay with the AC Stark Effect.

Our MBE-grown sample consists of a 20-period MQW with 80Å $In_{0.2}Ga_{0.8}As$ wells separated by 150Å $GaAs$ barriers on a $GaAs$ substrate. The energy of the 2D MQW states is below the substrate band-gap, allowing us to perform direct transmission spectroscopy without substrate removal. Strain lifts the valence-band degeneracy at $k = 0$, splitting the light-hole and heavy-hole bands by 50meV. The electron-heavy-hole exciton is the lowest-energy feature. It is inhomogeneously broadened by interface roughness and alloy disorder [9] with a FWHM of 6meV. The exciton $1s \rightarrow 2p$ transition energy ($\hbar\omega_{12}$) is 8meV, estimated from magneto-transmission experiments [8].

A CW Ti:Sapphire laser provides tunable near-bandgap radiation, in the near infrared (NIR), focused to a 200 μm spot. Its transmission is detected by a conventional SiPbN photo-diode, and peak NIR intensity is 100mW/cm². THz radiation is provided by the UCSB

Free-Electron Laser, a source of intense, coherent radiation tunable from $\hbar\omega_{\text{THz}} = 0.5\text{--}20\text{ meV}$ [10]. It is roughly collinear with the NIR beam and focussed to a $0.5\text{--}2.5\text{ mm}$ spot coincident with the NIR focus (Fig. 2c). We measure transmission spectra as a function of THz intensity and frequency. All measurements are performed in He vapor at 4 K .

We observe two distinct regimes of experimental behavior for different ranges of THz frequency, ω_{THz} . When ω_{THz} is less than ω_{12} , we observe a red-shift of the exciton for low THz intensities, i.e., an AC Stark shift. As THz intensity increases, this shift reaches a maximum and reverses, eventually becoming a net blue-shift at the highest THz intensity; the DFKE blue-shift dominates at high intensities as the AC Stark Effect saturates (Fig. 3a). Conversely, if ω_{THz} is greater than ω_{12} , we observe a blue-shift of the exciton which increases monotonically with increasing THz intensity; the AC Stark Effect and DFKE act in concert, each contributing to the blue-shift (Fig. 3b). In both cases, the exciton peak is broadened and suppressed, and the broadening increases with increased THz intensity (Fig. 3a, b).

Since the apparent peak shifts are small, we quantify them by taking a weighted average of the data near the exciton line. We find the geometric mean of the upper half of the excitonic peak, and plot this "center of mass" against ω_{THz} , which is directly proportional to THz power (Fig. 4). Note that our estimates of the maximum ω_{THz} at each frequency are only accurate to within a factor of 2 or 3. We also show results of our theoretical calculations (to be discussed below). Again, we see an initial red-shift, followed by a blue-shift at low ω_{THz} (Fig. 4a) and a monotonic blue-shift at high ω_{THz} (Fig. 4b).

Theoretically, we describe the optical properties of the system by calculating the time dependent induced polarization. The system is probed using a weak NIR probe field $E_{\text{NIR}}(t)$ with frequency ω . To linear order in the NIR field, the macroscopic polarization is the \mathbf{k} -trace of

$$\mathbf{P}(\mathbf{k}; t) = \sum_{\mathbf{k}'} \int_{-\infty}^t dt' \chi(\mathbf{k}; t, t') E_{\text{NIR}}(\mathbf{k}'; t') \quad (3)$$

All the information about the THz field is contained in the non-equilibrium generalization of the retarded two-time interband susceptibility $\chi(\mathbf{k}; t, t')$. In our previous work [5], based on non-equilibrium Green functions, we studied the susceptibility starting from a two-band Hamiltonian, including the THz field non-perturbatively in the Coulomb-gauge via the vector potential $\mathbf{A}(t) =$

$E_{\text{THz}} \sin(\omega_{\text{THz}} t) \hat{\mathbf{z}}$. Here, E_{THz} is oriented in the plane of the MQW layers. Non-equilibrium Green function techniques [12] yield an analytic expression for the single particle susceptibility:

$$\chi(\mathbf{k}; t, t') = \frac{2d^2}{\hbar} \langle t | \hat{\mathbf{z}} | t' \rangle \sin \left(\frac{\omega_{\text{THz}}}{2} (t - t') \right) \frac{ds}{\hbar} [\mathbf{k} - \mathbf{k}'] \quad (4)$$

where d is a dipole matrix element and $\mathbf{k} = \frac{\hbar \mathbf{k}}{2} + E_{\text{gap}}$, being the electron-hole reduced mass and \mathbf{k} the in-plane momentum.

We include excitonic effects by using the Bethe-Salpeter equation [11] to determine a susceptibility which includes the electron-hole interaction in the ladder approximation:

$$\chi(\mathbf{k}; t, t') = \chi(\mathbf{k}; t, t') + \frac{d^2 \mathbf{k}^0}{(2\pi)^2} \int_{-\infty}^t dt'' \chi(\mathbf{k}; t, t'') V(\mathbf{k} - \mathbf{k}^0) \chi(\mathbf{k}^0; t'', t') \quad (5)$$

where $\chi(\mathbf{k}; t, t')$ is the single-particle, non-interacting susceptibility of Eq. (4). Expressing the susceptibility as $\chi(\mathbf{k}; t, t') = \sum_n \frac{d_n}{2} \chi_n(\mathbf{k}; !) e^{i!(t-t') + i n \omega_{\text{THz}}(t+t')}$, the integralequation (5) becomes a matrix equation [13],

$$\begin{aligned} \chi_n(\mathbf{k}; !) &= \chi_n(\mathbf{k}; !) \\ &+ \sum_{n'} \frac{d_n d_{n'}}{(2\pi)^2} V(\mathbf{k} - \mathbf{k}^0) \chi_{n'}(\mathbf{k}^0; ! + 2(n - n')\omega_{\text{THz}}) \end{aligned} \quad (6)$$

For physically achievable THz intensities, only small values of n are needed.

Numerically, we solve the matrix equation including both s-wave and p-wave scattering; both are important, since the THz field will couple the s and p states of the exciton and induce the observed resonance via the AC Stark Effect. The solutions to the resulting equation are found by discretizing the integrals to yield a set of linear equations which we solve by standard methods [14].

Finally, we relate the results to physically measurable quantities by expressing the macroscopic polarization as

$$\mathbf{P}(t) = E_{\text{NIR}} \sum_n \tilde{\chi}_n(!) e^{i(2n\omega_{\text{THz}} + !)t} \quad (7)$$

where $\tilde{\chi}_n(!) = \sum_{\mathbf{k}} \chi_n(\mathbf{k}; !)$. The linear absorption is thus proportional to $\text{Im} \tilde{\chi}_0(!)$. The terms with $n \neq 0$ describe the non-linear mixing of the NIR and the THz field, resulting in optical sideband generation. These sidebands show a rich structure, but an analysis is beyond the scope of this work, and will be reported separately.

Using the above method, we have calculated absorption spectra using the experimental parameters of our system. We find good agreement with experiment, using no fitted parameters. For $\omega_{\text{THz}} < \omega_{12}$, theory predicts a red-shift of the exciton absorption peak at low THz intensities. With increasing THz intensity, the shift saturates and then reverses, eventually becoming a net blue-shift (Fig. 5a). Theory also predicts a blue-shift for $\omega_{\text{THz}} > \omega_{12}$, which monotonically increases with THz intensity for experimentally-accessible intensities (Fig. 5b). In both cases, the exciton peak is suppressed and inhomogeneously broadened with increasing intensity, i.e., with increasing ω_{THz} (Fig. 5ab). Using the same method as for

the measured spectra, we compute the "center of mass" of the calculated exciton lines. We plot the shift of the theoretical "center of mass" as a function of ω in Fig. 4, along with the experimental results. The theoretical and experimental peak shifts show identical qualitative behavior.

As described above, this behavior can be understood as the DFKE acting in competition with the AC Stark Effect. The AC Stark Effect, at low E_{THz} , results in a shift of the exciton level,

$$\propto \frac{(\omega_{THz} - \omega_{12})E_{THz}^2}{(\omega_{THz} - \omega_{12})^2 + \frac{\gamma^2}{2}}; \quad (8)$$

where γ is the width of the $1s \rightarrow 2p$ transition line [7]. We estimate $\hbar\gamma \approx 4$ meV in our sample. The magnitude of γ is dominated by γ_{12} , and we expect little resonant enhancement of γ for $\omega_{THz} \approx \omega_{12}$. γ does not increase indefinitely, and will saturate as E_{THz} increases, going from quadratic to linear dependence on E_{THz} [7]. The DFKE, however, always provides a blue-shift proportional to E_{THz}^2 , given by E_{KE} [5].

The net effect is illustrated in Figure 4, which shows the shift of the center of mass of the exciton transmission peak as a function of ω for both theory and experiment. For $\omega_{THz} < \omega_{12}$, we see a red shift which saturates and reverses with increasing intensity, showing a roughly linear dependence on THz intensity at high fields (Fig. 4a). At low fields, γ dominates, resulting in a net red shift. As γ saturates with increasing field, E_{KE} begins to dominate, eventually overwhelming the red shift entirely and resulting in a net blue shift. For $\omega_{THz} > \omega_{12}$, we observe only an increasing blue-shift with increasing E_{THz} (Fig. 4b). Here, γ and E_{KE} cooperate to create a blue-shift.

In conclusion, we have observed the experimental signature of DFKE through its interplay with the AC Stark Effect. Our theory and observations are in remarkable agreement, and show the resulting frequency- and intensity-dependent shift of the excitonic resonance in a MQW under intense THz irradiation.

This work is supported by ONR grant N00014-92-J-1452, the Quantum Transition Project of JSTC, QUEST (an NSF Science & Technology Center), LACOR grant no. 4157U0015-3A from Los Alamos National Laboratory, National Science Foundation grant CDA 96-01954, and by Silicon Graphics, Inc. The authors also wish to thank D.P. Enyeart, D.T. White, J.R. Allen and G. Ramian at the Center for Terahertz Science & Technology for their invaluable technical support.

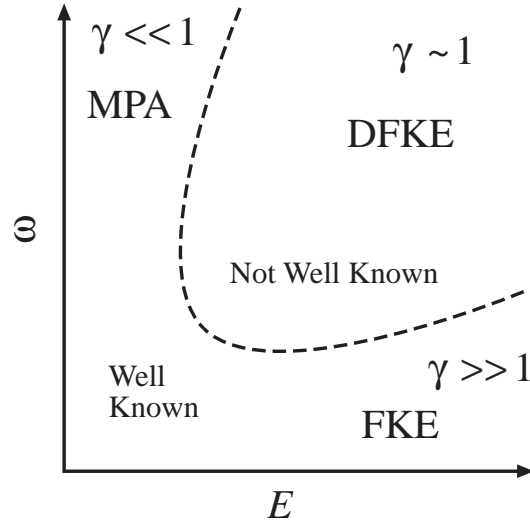


FIG. 1. A schematic map of electro-optic phase space as a function of amplitude and frequency of the perturbing field, showing DFKE regime "between" MPA and FKE.

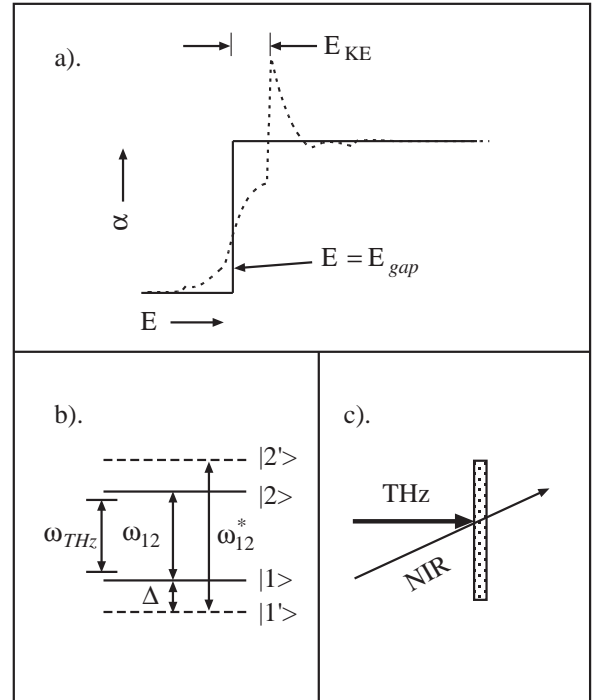


FIG. 2. (a) DFKE in an ideal 2D system. In a strong THz field (dashed curve, solid curve is zero-field), the "edge" shifts to higher frequency and sub-gap absorption increases. (b) The AC Stark Effect: a strong field applied at frequency $\omega \approx \omega_{12}$ causes ω_{12} to shift. For $\omega < (>) \omega_{12}$, the transition shifts to $\omega_{12} > (<) \omega_{12}$. $\Delta = (\omega_{12} - \omega_{12}')/2$ is the shift of ω_{12} with respect to distant energy levels. (c) Schematic of experiment.

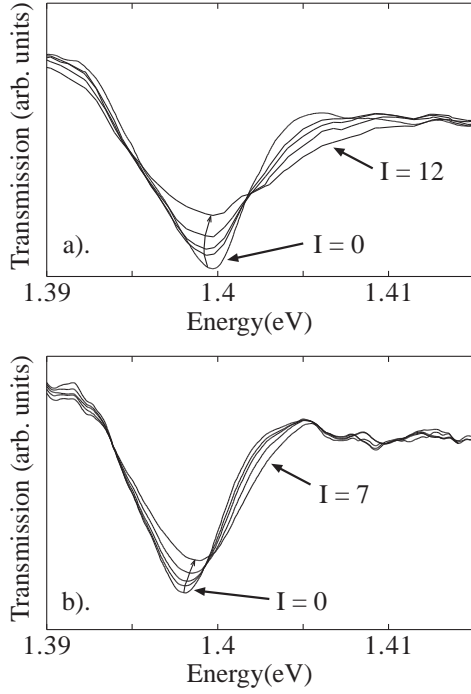


FIG. 3. Experimental transmission of MQW near the 1st exciton with (a) $h\nu_{\text{THz}} = 2.5 \text{ meV}$ at $I_{\text{THz}} = 0; 1; 2; 4; 12$ (arb. units). (b) $h\nu_{\text{THz}} = 14 \text{ meV}$ at $I_{\text{THz}} = 0; 1; 2; 4; 7$ (arb. units). Arrows connect calculated centers of experimental peaks and point in direction of increasing I_{THz} .

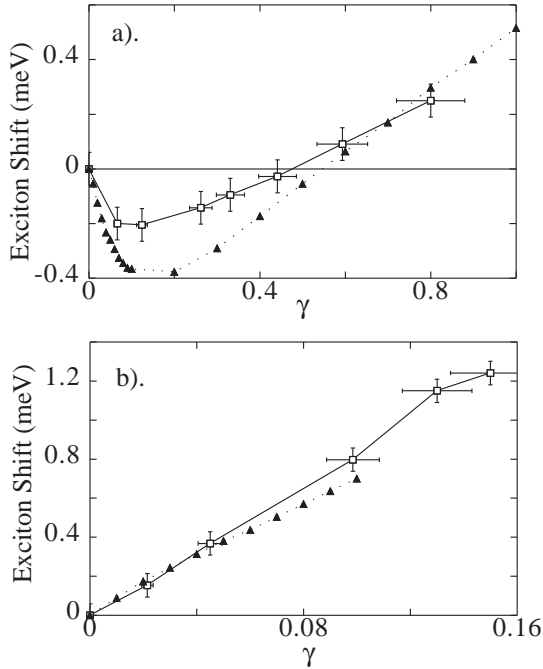


FIG. 4. "Center of mass" of measured (squares) and calculated (triangles) exciton transmission peak vs. γ for (a) $h\nu_{\text{THz}} = 2.5 \text{ meV} < h\nu_{12}$ (b) and $h\nu_{\text{THz}} = 10.5 \text{ meV} > h\nu_{12}$.

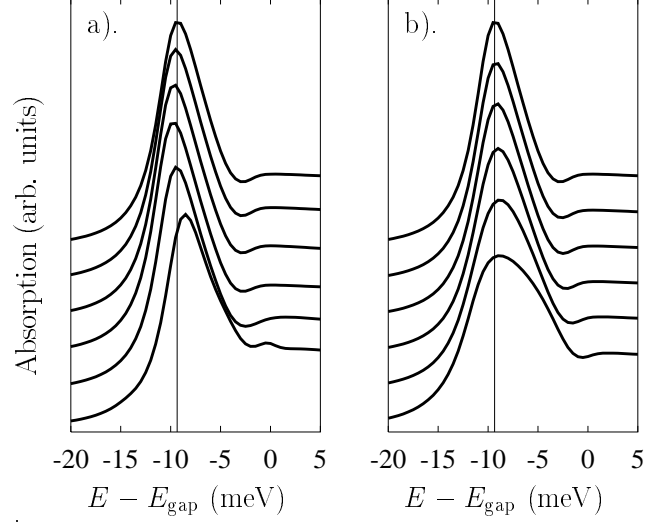


FIG. 5. Calculated absorption of MQW with; (a) $h\nu_{\text{THz}} = 2.5 \text{ meV} < h\nu_{12}$ from top down at $\gamma = 0, 0.03, 0.06, 0.1, 0.5, 1.5$. (b) $h\nu_{\text{THz}} = 14 \text{ meV} > h\nu_{12}$ from top down at $\gamma = 0, 0.01, 0.02, 0.04, 0.08, 0.15$.

-
- [1] W. Franz, Z. Naturforschung 13, 484 (1958).
 - [2] L. V. Keldysh, Sov. Phys. JETP 34, 788 (1958).
 - [3] See, e.g., V. Nathan, A. H. Guenther, and S. S. Mitra, J. Opt. Soc. Am. B 2, 294 (1985) and references therein.
 - [4] Y. Yacoby, Phys. Rev. 169, 610 (1968).
 - [5] A. P. Jauho and K. Johnsen, Phys. Rev. Lett. 76, 4576 (1996); K. Johnsen and A. P. Jauho, Phys. Rev. B 57, 8860 (1998).
 - [6] Y. T. Rebane, Sov. Phys. Solid State 27, 824 (1985).
 - [7] See, e.g., J. S. Bako, Physics Reports 31C, 209 (1977) and references therein.
 - [8] J. Kono et al, Phys. Rev. Lett. 79, 1758 (1997).
 - [9] A. Patane et al, Phys. Rev. B 52, 2784 (1995).
 - [10] G. Ramian, Nucl. Inst. and Meth. A 318, 225 (1992).
 - [11] H. Haug and S. Schmitt-Rink, Progress in Quantum Electronics, 9, 1, (1984).
 - [12] H. Haug and A. P. Jauho, Quantum Kinetics in Transport and Optics of Semiconductors (Springer, Berlin, 1996).
 - [13] K. Johnsen and A. P. Jauho, (unpublished).
 - [14] H. Haug and S. W. Koch, Quantum theory of the optical and electronic properties of semiconductors (World Scientific, Singapore, 1993).